International Journal of the Physical Sciences Vol. 5(17), pp. 2622-2634, 18 December, 2010
Available online at http://www.academicjournals.org/IJPS
ISSN 1992-1950 ©2010 Academic Journals

Full Length Research Paper

Material properties of air-cured ultra-high-performance steel-fiber-reinforced concrete at early ages

Ki Nam Hong[1]*, Su Tae Kang[2], Sung Wook Kim[2], Jung Jun Park[2] and Sang Hoon Han[1]

[1]Department of Civil Engineering, Chungbuk National University, San 12, Gaesin-dong, Cheongju-si, Chungbuk-do, 361-763, South Korea.
[2]Department of Structural Material, Korea Institute of Construction Technology, 2311, Daehwa-dong, Ilsanseo-gu, Goyang 411-702, South Korea.

Accepted 26 November, 2010

This study investigated the material properties of air-cured ultra-high-performance fiber-reinforced concrete (UHPFRC) at early ages. To assess the material properties of UHPFRC at early ages, compressive and three-point bending tests were respectively performed at the 10 stages of early ages on ø 100 × 200 mm cylinders and 100 × 100 × 400 mm specimens made from UHPFRC with a 2% steel fiber volume ratio. Based on the regression analysis of the compressive and flexural test results for each age, model equations were proposed that can predict the compression strength, modulus of elasticity and flexural strength at early ages. In addition, to determine the tensile softening curves of UHPFRC at early ages, the inverse finite element (FE) analysis was applied using the poly-approximation method; based on the results, model equations are presented that can predict the tensile softening curve. The load-variable curves obtained from the simulation using the proposed tensile softening model fit the measurements from the flexural tests relatively well.

Key words: UHPFRC, air curing, material property, tensile softening, early age.

INTRODUCTION

Ultra-high-performance fiber-reinforced concrete (UHPFRC) is a very special material with superior mechanical properties and low permeability. The high strength and strain-hardening behavior under tensile loading let this material resist serious loads and extreme environmental conditions. Along with the superior strain-hardening behavior, the dense matrix endows UHPFRC with a very low permeability, which is the main reason for UHPFRC having high durability compared to ordinary concrete materials (Richard et al., 1995; Rossi et al., 2005; Bache, 1987; Charron et al., 2004; Lawler et al., 2002). UHPFRC is generally produced through high-temperature curing. Although the high-temperature curing process reduces the curing time for UHPFRC and increases early strength (Urs et al., 2008), it is not only highly energy consuming and uneconomical but also the main cause of limiting the use of UHPFRC to mostly factory products.

Normal-temperature curing has been assumed to greatly reduce material properties of UHPFRC at early ages. However, a number of studies have shown that UHPFRC cured at a normal temperature showed not only the development of superior long-term strength but also outstanding practicality (Fehling et al., 2004; Parant, 2003). Fehling et al. (2004) investigated the compression strength of high- and normal-temperature-cured ultra-high-performance concrete (UHPC) for several ages. They reported that the strength increases of normal- and high-temperature-cured concrete between 7 and 56 days were 40 and 10%, respectively. Parant et al. (2003) reported that, the strength of high-temperature-cured UHPFRC increased by 5% between 28 and 200 days and by an additional 5% between 200 and 400 days, while that of air-cured UHPFRC increased by 5% between 35 and 91 days and by an additional 10% between 91 and 400 days. The development of material properties is the basis for the design and construction of structures made from cement-based materials. Cracks appearing at early

*Corresponding author. E-mail: hong@chungbuk.ac.kr.

Table 1. Mix design of UHPFRC.

Cement content (kg/m^3)	Relative weight ratios to cement						Steel fiber (Vf, %)*
	Cement	Water	Silica fume	Fine aggregate	Filler	Superplasticizer	
821.7	1.00	0.25	0.25	1.10	0.30	0.018	2

* Fiber volume expressed as volumetric ratio to the whole volume

Table 2. Physical and chemical properties of cement and silica fume.

Material	Specific surface area (cm^2/g)	Density (g/cm^3)	Chemical composition (%)					
			SiO_2	Al_2O_3	Fe_2O_3	CaO	MgO	SO_3
OPC	3,413	3.15	21.01	6.40	3.12	61.33	3.02	2.3
Silica fume	200,000	2.10	96.00	0.25	0.12	0.38	0.1	-

Table 3. Properties of fresh UHPFRC.

Flow (mm)	Slump flow (mm)	Air content (%)	Unit weight (kg/m^3)	Setting time (h)	
				Initial set	Final set
205	590	3.9	2,484	13.3	15.8

ages have a very close relationship with tensile strength. In particular, the manifestation of tensile strength at early ages has a great impact on form removal or the pre-stressing construction process. In addition, development of tensile strength at an early age has a very desirable effect on the load-carrying capacity or stiffness of structures (Katrin et al., 2006).

However, studies on the material properties of UHPFRC have been done by only a small number of researchers (Tanaka et al., 2005; Kang et al., 2010). In particular, there are no studies on the material properties of air-cured UHPFRC at early ages that has been placed onsite. Therefore, this study aimed to investigate the material properties of air-cured UHPFRC at an early age through experiments and to use the results to develop a material model that can predict the material properties of UHPFRC at early ages.

EXPERIMENTAL PROGRAM

Materials

The UHPFRC mix design differs greatly from the design of normal and high-strength concrete. The composition of UHPFRC is characterized by high cement, high-range water reducer, and silica fume content. The UHPFRC mix design applied in the present study is presented in Table 1. The cement used in the mix was normal Portland cement. The water-to-binder ratio (w/b) was 2, and a large amount of silica fume equal to 25% of the cement weight was used. The physical and chemical properties of the cement and silica fume used in the present study are presented in Table 2.

For the aggregate, aggregates A (density: 2.62 g/cm^2, average grain diameter: 0.3 to 0.5 mm, SiO_2 93%) and B (density: 2.62 g/cm^2, average grain diameter: 0.17 to 0.3 mm, SiO_2 93%) mixed at a 7:3 ratio were used. To obtain sufficient strain-hardening behavior, steel fiber corresponding to a 2% volume ratio was intermixed. The tensile strength, diameter, and length of the steel fiber used in the mix were 2,500 MPa, 0.2 and 13 mm, respectively. In addition, siliceous filler was used to improve early age strength and durability. In addition, the properties of fresh UHPFRC is presented in Table 3.

Experiment process

In this study, compression and flexural tests were performed to investigate the material properties of air-cured UHPFRC at early ages. The tests were done in 10 stages at the ages of 0.83, 1.00, 1.25, 1.50, 2.00, 2.50, 3.00, 7.00, 14.0, and 28.0 days. The tests were first done at the age of 0.83 day because prior to that point, the concrete had not hardened, which made mold removal almost impossible. Identical tests were performed on high-temperature-cured specimens at the age of 28 days, and the material properties depending on curing methods were compared. The high-temperature curing was done at 90℃ for 3 days.

For the compressive test, ø100 × 200 mm cylinders generally chosen for compressive tests were used. Since grinding was impossible at ages before 1.25 days, capping was done by using ultrathin cement; for ages thereafter, both ends of the cylinders were polished. Compressive tests were done by using a universal testing machine with a capacity of 3,000 kN. The load was measured by using a 3,000-kN-capacity load cell. The cylinder displacement was measured by using a compression meter composed of three LVDTs. The loading was applied through the displacement control method at a rate of 0.003 mm/s. The overall view of the compressive test apparatus setup is shown in Figure 1.

The three-point flexural tests were performed on 100 × 100 × 400 mm specimens generally used in flexural tests. A total of 60 specimens (six at each age) were prepared. Of the six specimens

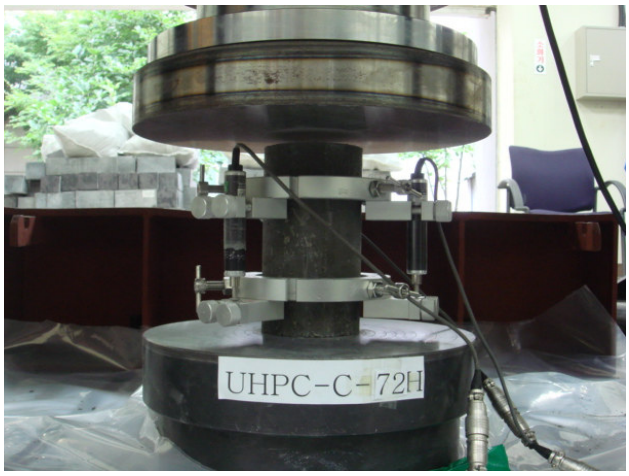

Figure 1. Overall view of compressive test setup.

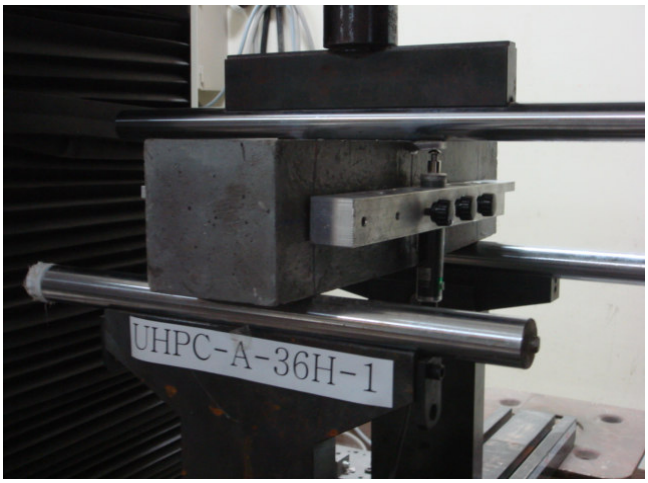

Figure 2. Overall view of three-point bending test setup.

at each age, flexural tests were done on three without notches. For the remaining three specimens, a notch was cut at the center of each specimen prior to the tests. The width and height of the notch were fixed at 4 and 30 mm, respectively. A 2,000-kN-capacity UTM was used in the flexural tests. Displacement control loading at the rate of 1/1,500 of the net specimen span per min was applied. To measure the displacement of the specimen's center during the testing, two LVDTs with 10.0-mm capacity were installed, one on each side. In addition, to measure the crack width in the notch, a 5-mm-range clip gauge was attached to the bottom of the specimen. The overall view of the setup and the schematic diagram of the three-point bending test are presented in Figures 2 and 3, respectively.

TEST RESULTS

Compressive test

The compressive stress-strain curves obtained at each

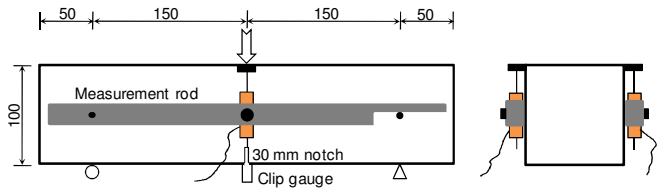

Figure 3. Schematic diagram of three-point bending test (unit: mm).

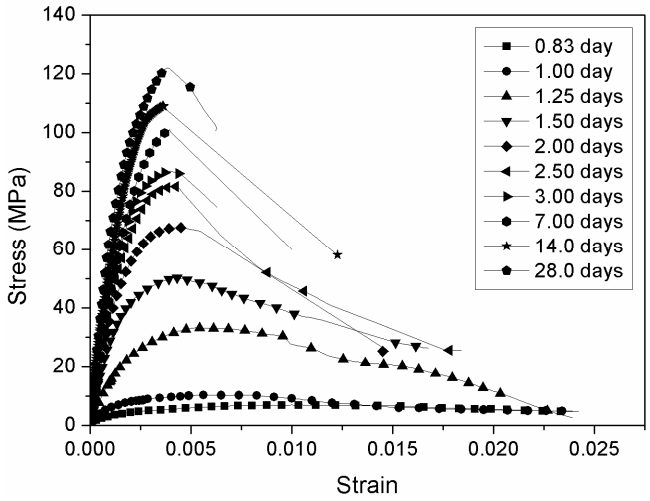

Figure 4. Compressive stress-strain curves with respect to age.

age are shown in Figure 4. These curves represent the averages from the results of three cylinders at each age. At early ages after casting, a low modulus of elasticity, low strength, and very high strain corresponding to the maximum strength are exhibited. However, as the age increases, the modulus of elasticity and compressive strength increase rapidly, while the strain corresponding to the maximum strength tends to decrease quickly. Figure 4 verifies that the stress-strain curve changed rapidly after 1.25 days following casting. Figure 5 shows the compressive stress-strain curves of the high-temperature-cured cylinder and 28-day air-cured cylinder. When compared, the compressive strength and modulus of elasticity of the 28-day air-cured specimens were shown to be 64 and 84%, respectively, of those of the high-temperature-cured cylinders; this confirms that the curing method has a very large impact on compression capacity.

To formulate the compressive strength f_c and the modulus of elasticity E_c of UHPFRC, regression analyses were performed on the test results. Equations (1) and (2) are proposed formulas for predicting the compressive strength f_c and modulus of elasticity E_c of air-cured UHPFRC at early ages as obtained from the

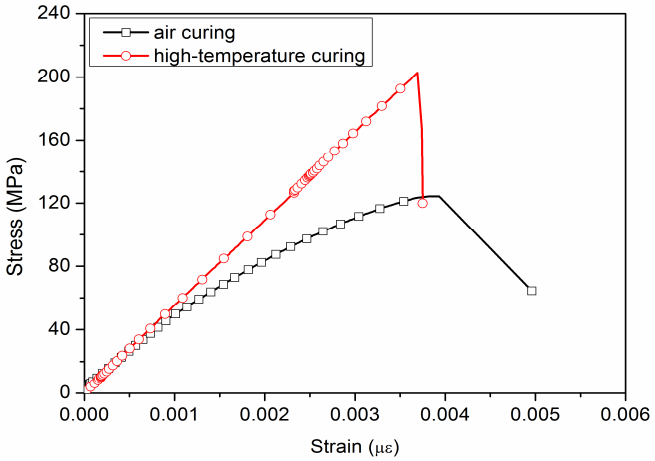

Figure 5. Compressive stress-strain curves with respect to curing method.

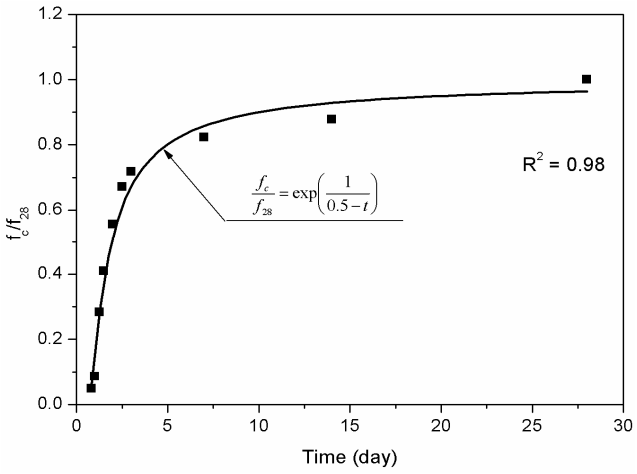

Figure 6. Relationship between f_c / f_{28} and time.

nonlinear regression analyses of the cylinder test results. The regression analyses were performed by using Origin 7.5 software (2003).

$$f_c = f_{28} \cdot \exp\left(\frac{1}{0.5-t}\right) \quad (1)$$

$$E_c = E_{28} \cdot \exp\left(\frac{0.4}{0.8-t}\right) \quad (2)$$

where t is in days and f_c, E_c, f_{28}, and E_{28} are in MPa. f_{28} and E_{28} are the compressive strength and elasticity of modulus, respectively, at 28 days. Figures 6 and 7 are the plots of f_c / f_{28} versus t and E_c / E_{28} versus t, respectively. Meanwhile, in Figures 6 and 7, R^2 represents the correlation coefficient.

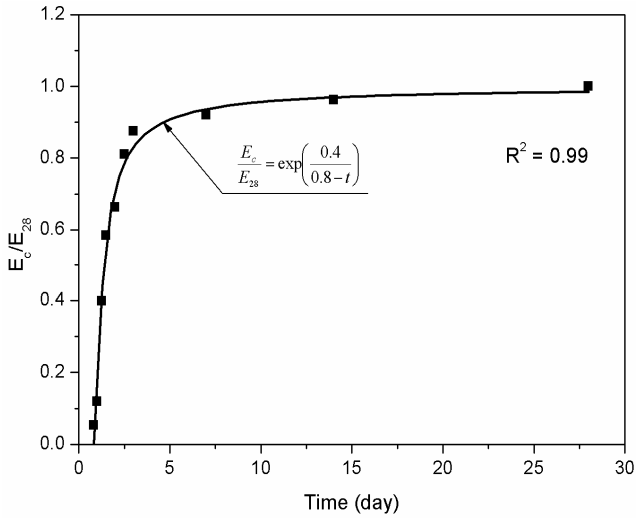

Figure 7. Relationship between E_c / E_{28} and time.

Bending tests

Figure 8 shows the typical crack patterns of non-notched and notched beams after the three-point flexural tests. The crack patterns confirm that the primary cracks occurred in the central sections of most beams, and steel fibers play an important role in bridging both crack surfaces. Due to the bridging mechanism of these fibers, UHPFRC can perform with very superior tensile capacity compared to UHPC, which lacks fibers. The flexural strengths obtained from the tests of the non-notched beams are presented in Table 4. The table shows that the flexural strength of air-cured UHPFRC rapidly increased up to the age of 3 days, and the strength after 7 days was not significantly different from that at 28 days.

To formulate the flexural strength f_t of air-cured UHPFRC, a regression analysis was done on the test results. Equation (3) was obtained from the nonlinear multiple regression analysis of the test results.

$$f_t = f_{t28} \cdot \exp\left(\frac{0.4}{0.8-t}\right) \quad (3)$$

where f_t and f_{t28} are in MPa. f_{t28} is the flexural strength at an age of 28 days.

Figure 9 is the plot of f_t / f_{t28} versus t. Figure 10 shows the load-displacement curves obtained from the

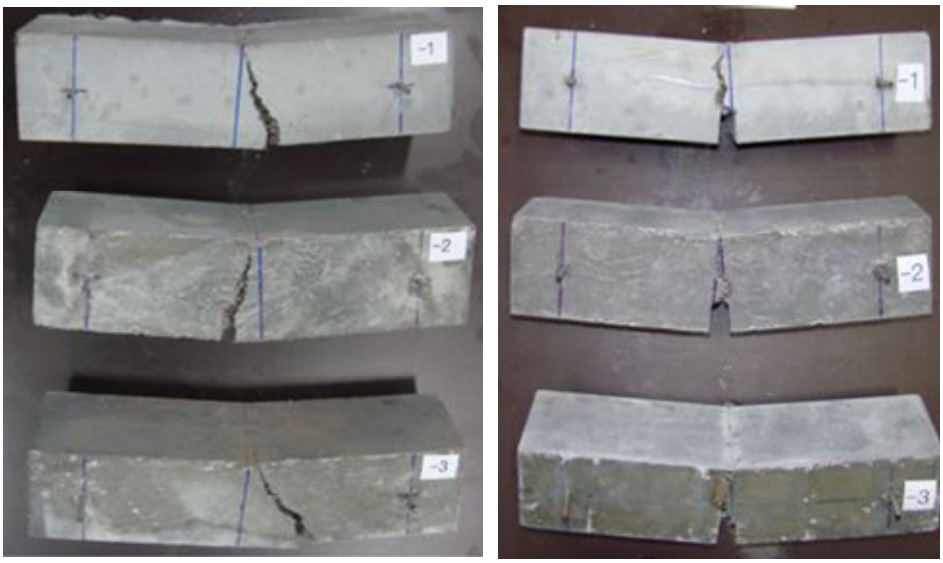

(a) non-notched beams (b) notched beams

Figure 8. Failure configuration after three-point bending test.

Table 4. Results of compressive and bending test.

Age (days)	Compressive strength (MPa)	Modulus of elasticity (N/mm^2)	Flexural strength (MPa)
0.83	7.07	2,407	1.40
1.00	10.70	5,471	5.25
1.25	35.20	18,367	14.85
1.50	50.92	26,875	16.29
2.00	68.17	30,522	20.47
2.50	85.70	37,322	23.03
3.00	89.32	40,258	23.37
7.00	102.42	42,333	25.18
14.0	110.82	44,333	28.03
28.0	126.88	46,034	28.76

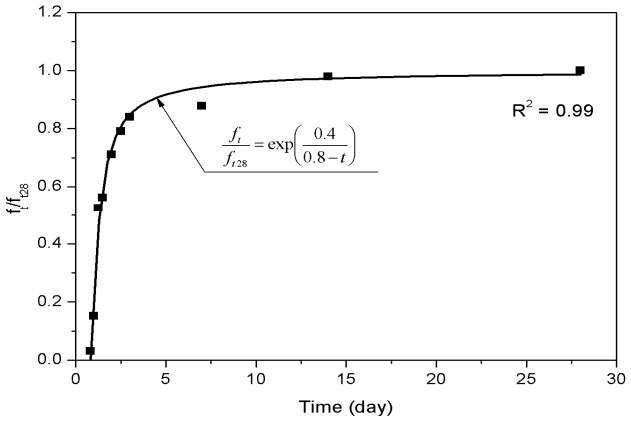

Figure 9. Relationship between f_t / f_{t28} and time.

notched beams at each age. As illustrated in Figure 10, a large scatter is shown between the load-displacement curves at earlier ages. The large scatter appearing at the earlier ages is thought to be due to the instability of the matrix. Figure 11 shows the comparison of the average load-displacement curves at each age. This figure shows that serious change does not occur in the initial stiffness with the increase in age, but in the post-peak region, behavior gradually becomes brittle. Figure 12 shows the comparison of the load-displacement curves of the high-temperature-cured beam and 28-day air-cured notched beam. The maximum loads of the high-temperature-cured beam and 28-day air-cured beam were 37.0 and 33.3 MPa, respectively, with the former having 11% greater load capacity. However, the behavior in the post-peak region showed no significant difference. Hence, compared

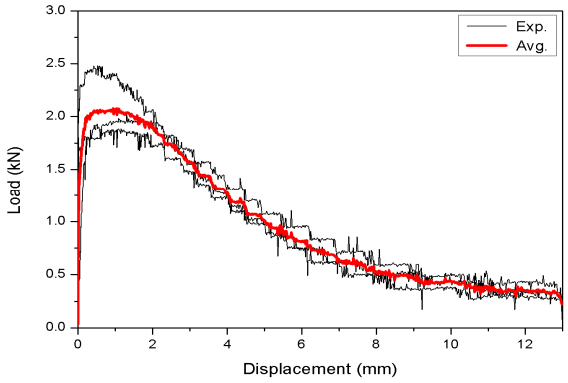

(a) 0.83 day

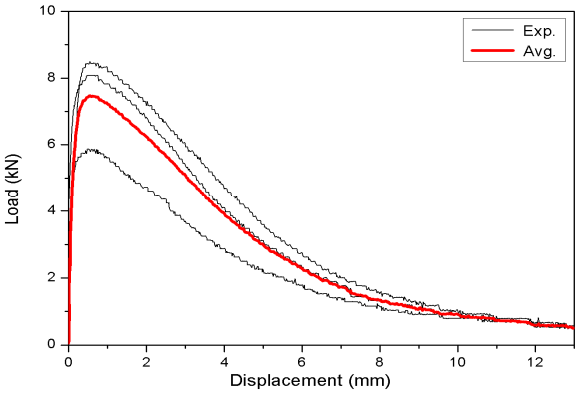

(b) 1.00 day

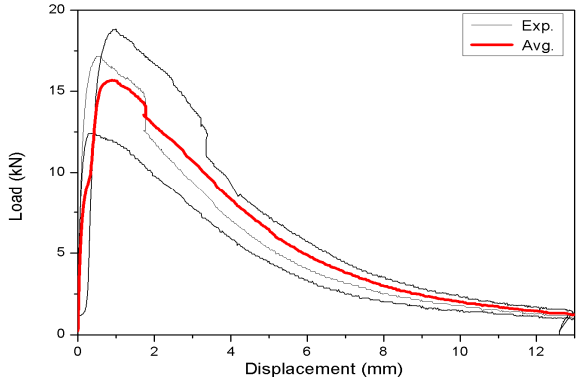

(c) 1.25 days

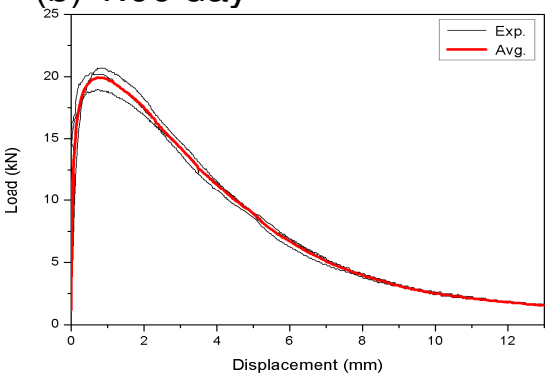

(d) 1.50 days

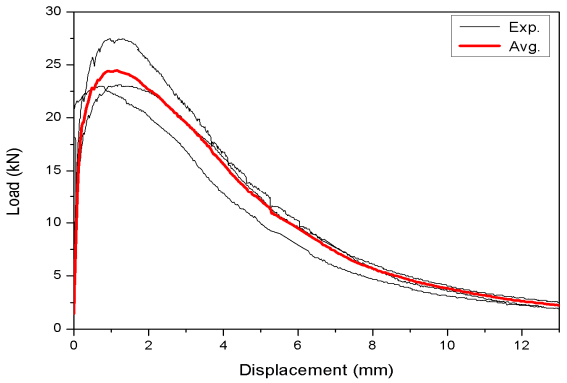

(e) 2.00 days

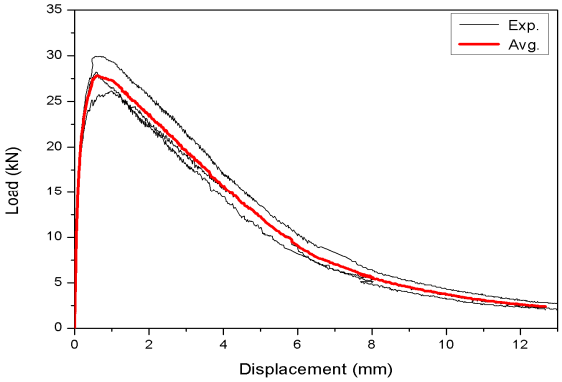

(f) 2.50 days

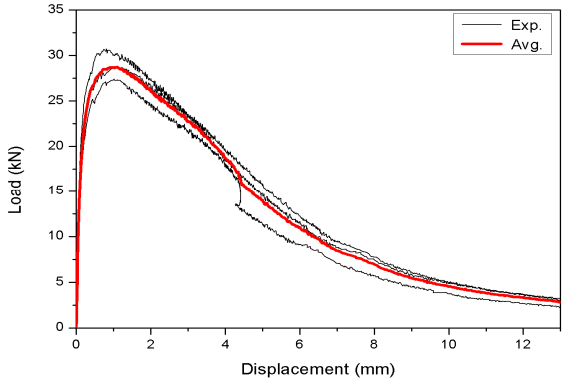

(g) 3.00 days

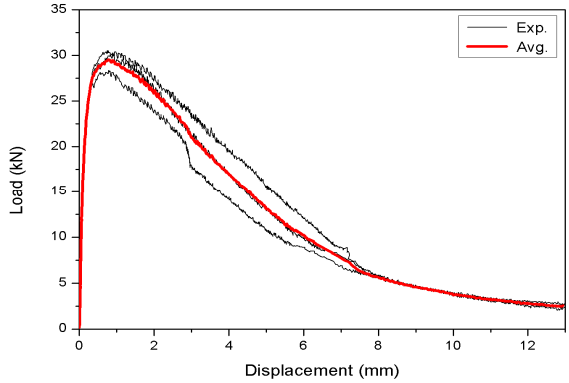

(h) 7.00 days

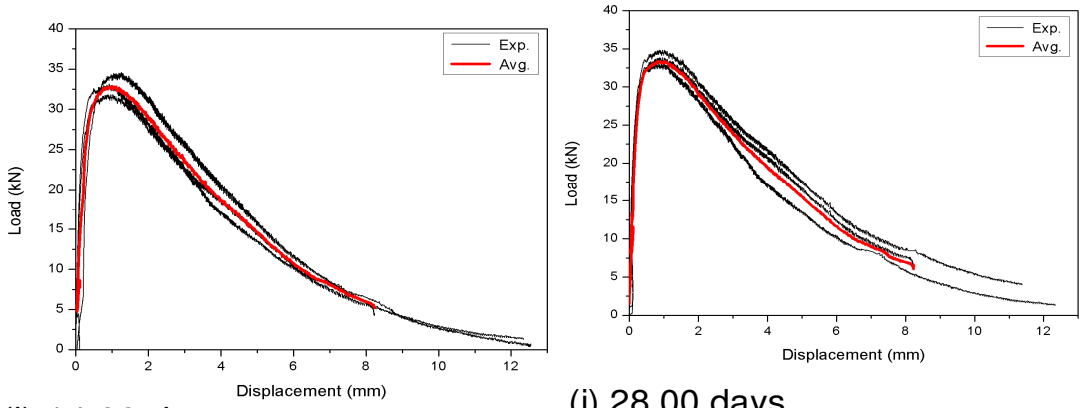

Figure 10. Bending load-displacement curves.

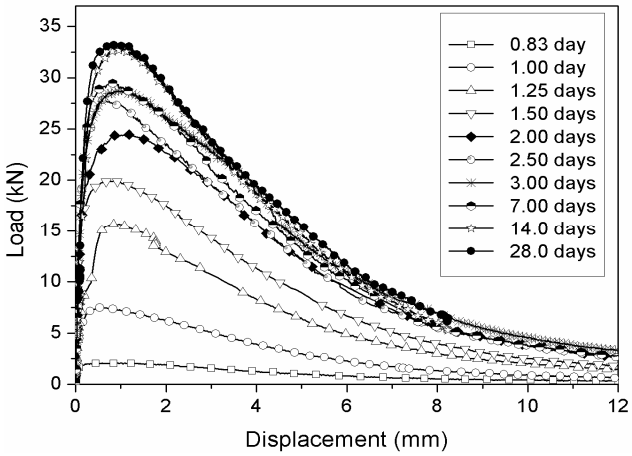

Figure 11. Bending load-displacement curves with respect to age.

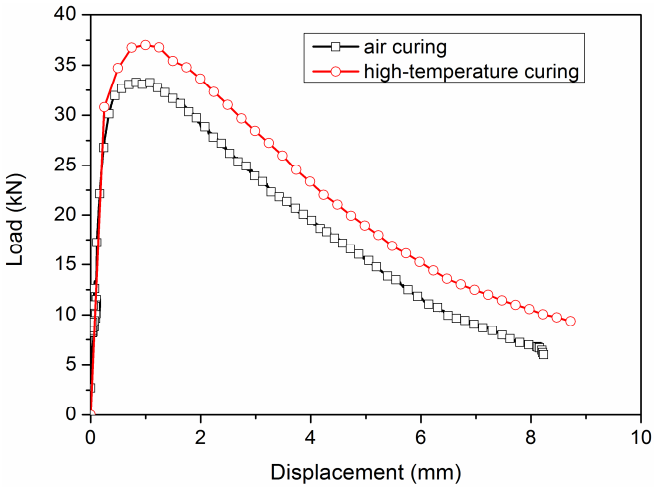

Figure 12. Bending load-displacement curves with respect to curing method.

to the compressive behavior, the difference in flexural behavior depending on the curing method was confirmed to be very insignificant. This is deemed to be because steel fibers have a greater primary impact on flexural behavior than on the compressive strength.

TENSILE SOFTENING MODEL OF AIR-CURED UHPFRC AT EARLY AGES

Inverse analysis process

Flexural strength is generally considered to be a very important tensile property in determining failure capacity. However, this property by itself is not sufficient for accurately revealing the failure mechanism of UHPFRC, which manifests superior tensile softening behavior due to the bridging effect. In contrast to UHPC without fibers, the fibers in UHPFRC play an important role in creating outstanding bridging stress between the crack surfaces. The bridging stress between the surfaces of cracks with wide openings is the main reason for the very high toughness and ductility of UHPFRC. Therefore, to accurately understand the crack occurrence and failure behavior of air-cured UHPFRC at early ages, the development of a tensile softening model that can accurately predict tensile softening behavior at early ages is essential.

In this study, the inverse analysis method proposed by Uchida et al. (1995) was applied to determine the tensile softening model for UHPFRC. This method is unique in that, it requires only the load-displacement data obtained from the flexural tests as input data. Moreover, this method performs the inverse analysis by using the finite element (FE) analysis, applying the fictitious crack model (FCM) and the modified poly-linear approximation method, to ultimately derive the crack opening displacement (COD). The inverse analysis method based on the poly-linear approximation method proposed by

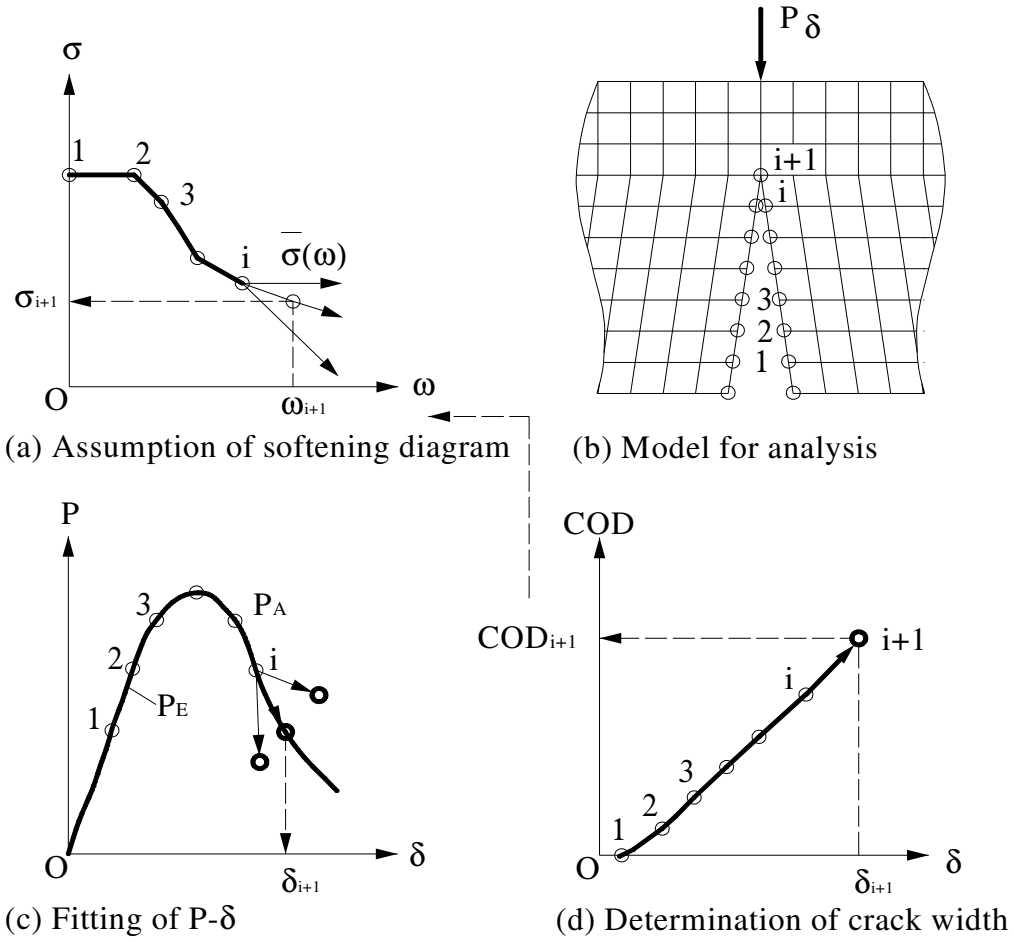

Figure 13. Modified poly-linear approximation method (Uchida et al., 1995).

Kitsutaka et al. (1993, 1995) was verified to have sufficient accuracy with respect to ordinary concrete. In addition, when applying it to fiber-reinforced concrete, which depends on the bridging characteristics of fibers rather than on the tensile strength of concrete, Uchida et al. modified the original poly-linear approximation method proposed by Kitsutaka et al. (1993, 1995), and Tanaka et al. (2005) and Kang et al. (2010) verified its accuracy with respect to UHPFRC.

Figure 13 explains the general concept of the modified poly-linear approximation method proposed by Uchida et al. (1995). They assumed that the initial region of the softening curve is perfectly plastic, as shown in Figure 13(a). In their method, the tensile strength is the stress when the relationship between the test and analytical load-displacements is within the allowed margin of the error range and the fictitious crack length is at its longest. The crack width at the endpoint of the perfect plastic section is the COP when the fictitious crack length is at its longest. The knee points past the perfect plastic section are determined by the original poly-linear approximation method. The performance of this method is outstanding because there is no need to assume the tensile softening curve in advance as the input value of the FE analysis program.

In this method, the softening curve can be constructed sequentially from the progressive optimization of the load-displacement curve, as shown in Figure 13. Since the post-crack behavior of UHPFRC cannot be fully determined because of the high strength of the matrix and the complex bridging mechanism of the fibers, the poly-linear approximation method is very effective in predicting the overall shape of the tensile softening curve. Figure 14 illustrates the overall procedure for deducing the tensile stress-crack width relationship through the inverse FE analysis based on the load-displacement results of the flexural tests. The FE model is composed of 740 nodal points and 1,393 triangular surface elements. The notch at the center of the specimens was modeled by using a dense mesh to accurately assess the crack growth. In the results for the inverse FE analysis, a curve given the name “primitive softening curve” was finally obtained. Subsequently, the primitive softening curve is simplified into a numerical model with two linear sections.

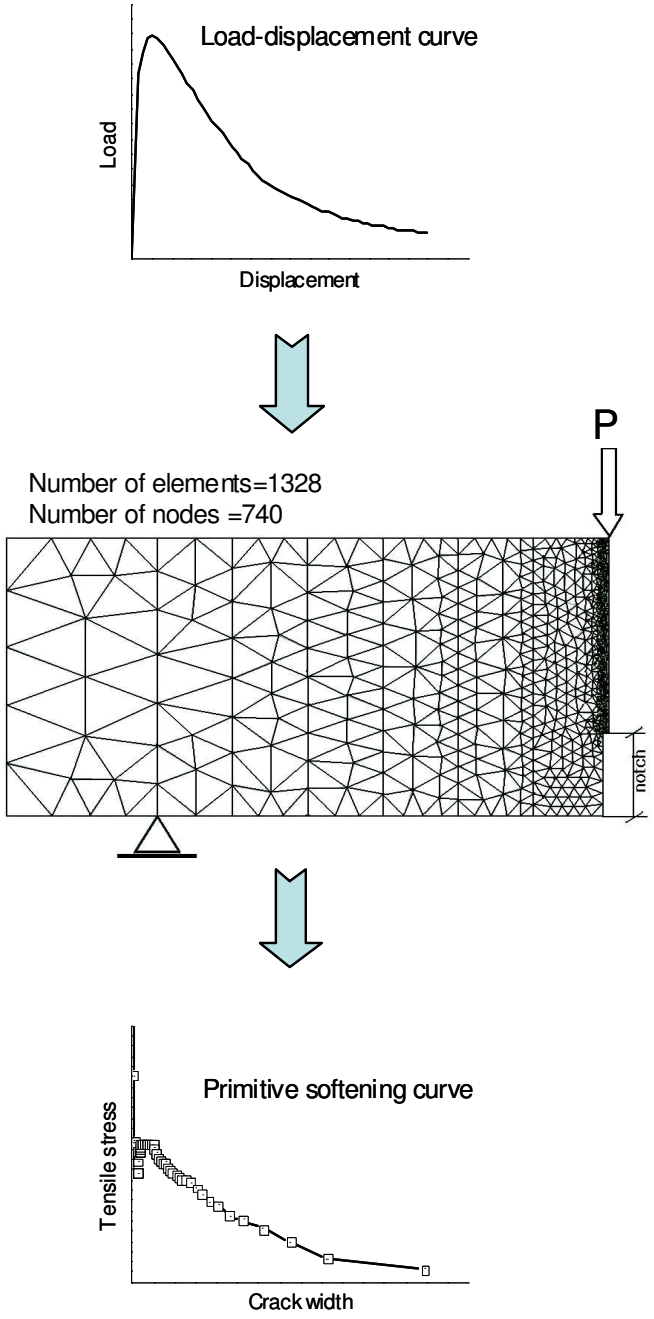

Figure 14. Procedure of inverse analysis (Kang et al., 2010).

Tensile softening curve formulation

As discussed earlier, the poly-linear approximation method deduces a discrete softening curve—termed here as a primitive softening curve—for UHPFRC through successive FE analyses. By using the primitive softening curve, it is possible to predict the original shape of the tensile softening curve for UHPFRC. Figure 15 shows the primitive softening curve obtained from the inverse analysis performed on the UHPFRC samples at 10 stages of age. Figure 16 displays the comparison of the

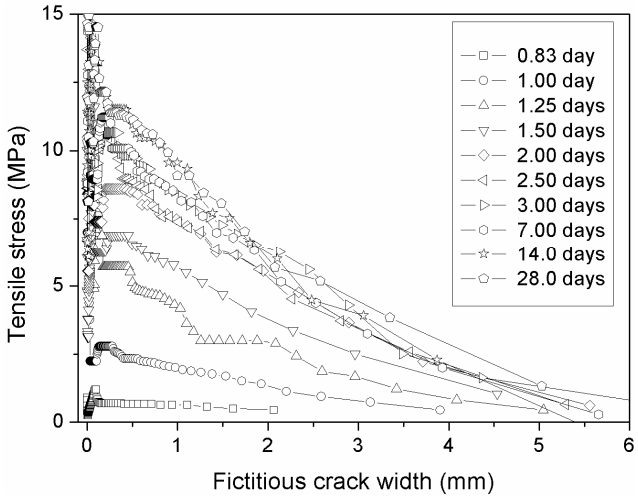

Figure 15. Tension-softening curves with respect to age.

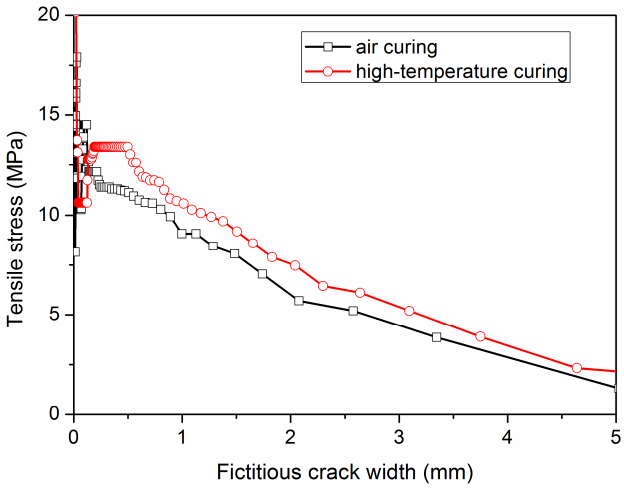

Figure 16. Tension-softening curves with respect to curing method.

primitive softening curves of high-temperature-cured and 28-day air-cured notched beams. This figure shows that there was no substantial difference in strain-softening behavior depending on the curing method.

Although the primitive softening curve in itself is the optimal solution obtained through the inverse analysis, because it is obtained in the form of a discrete solution, there are a few problems in directly applying it to the FE analysis or structure design. Hence, there is a need to show the primitive softening curve in a simplified form so that it can be applied in the nonlinear analysis, for determining structural behavior such as crack propagation and failure. In this study, the primitive softening curve, as illustrated in Figure 17, was simplified into two straight lines with a bridging plateau region and a softening region. As shown in Figures 18 to 20, a

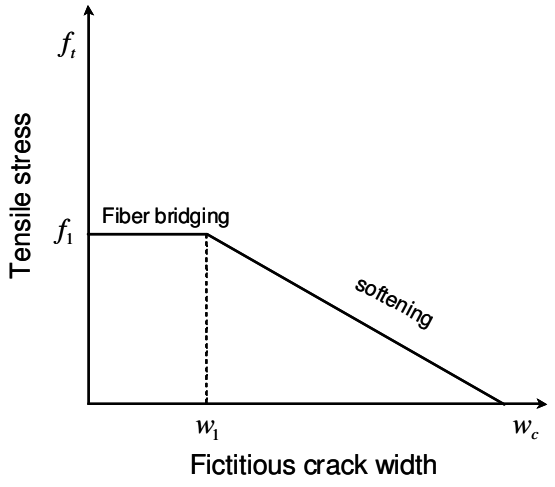

Figure 17. Modeled two-linear softening curve.

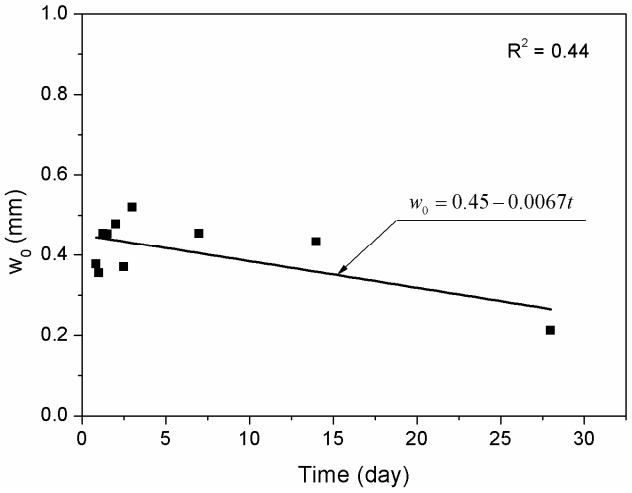

Figure 19. Relationship between w_1 and time.

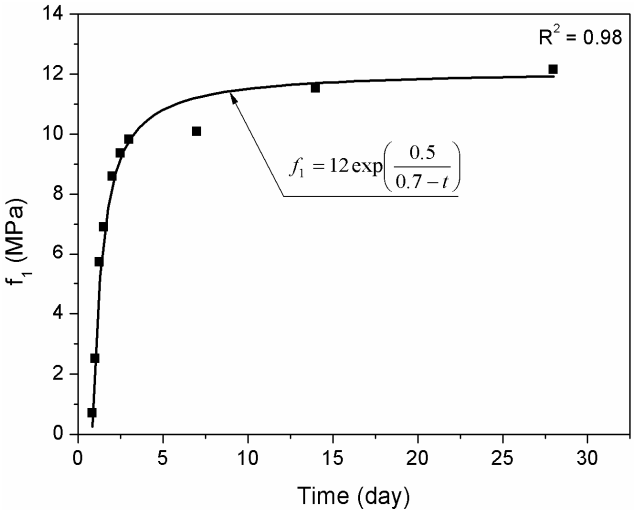

Figure 18. Relationship between f_1 and time.

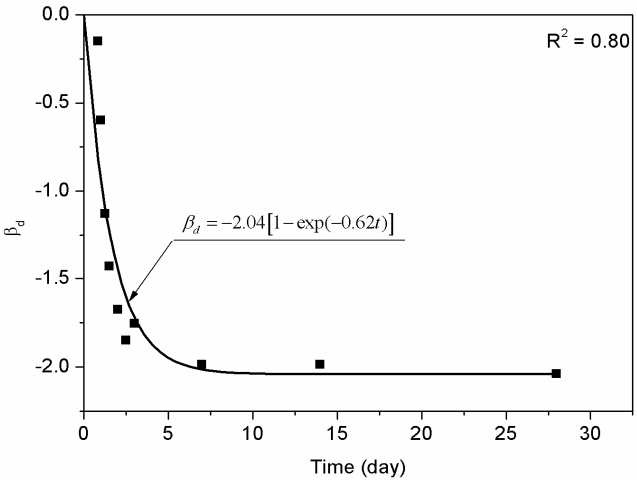

Figure 20. Relationship between β_d and time.

regression analysis was performed on the characteristic values of the primitive softening curve in order to formulate the tensile strength f_1, crack width w_1 at the endpoint of the bridging plateau region, and slope β_d of the softening region. Equations (4) and (6) are obtained from the nonlinear multiple regression analysis, and Equation (5) is obtained from the linear regression analysis.

$$f_1 = 12 \cdot \exp\left(\frac{0.5}{0.7-t}\right) \quad (4)$$

$$w_1 = 0.45 - 0.0067t \quad (5)$$

$$\beta_d = -2.04[1-\exp(-0.62t)] \quad (6)$$

$$w_c = \frac{f_1}{\beta_d} \quad (7)$$

where f_1, w_1, and w_c are in MPa, mm, and mm, respectively. Figures 18 to 20 show the plots of f_1 versus t, w_1 versus t, and β_d versus t, respectively.

In this paper, Equation (8) is finally proposed as the tensile softening model for air-cured UHPFRC at early ages.

$$\sigma_w = f_1 \text{ for } w \le w_1 \quad (8\text{-}1)$$

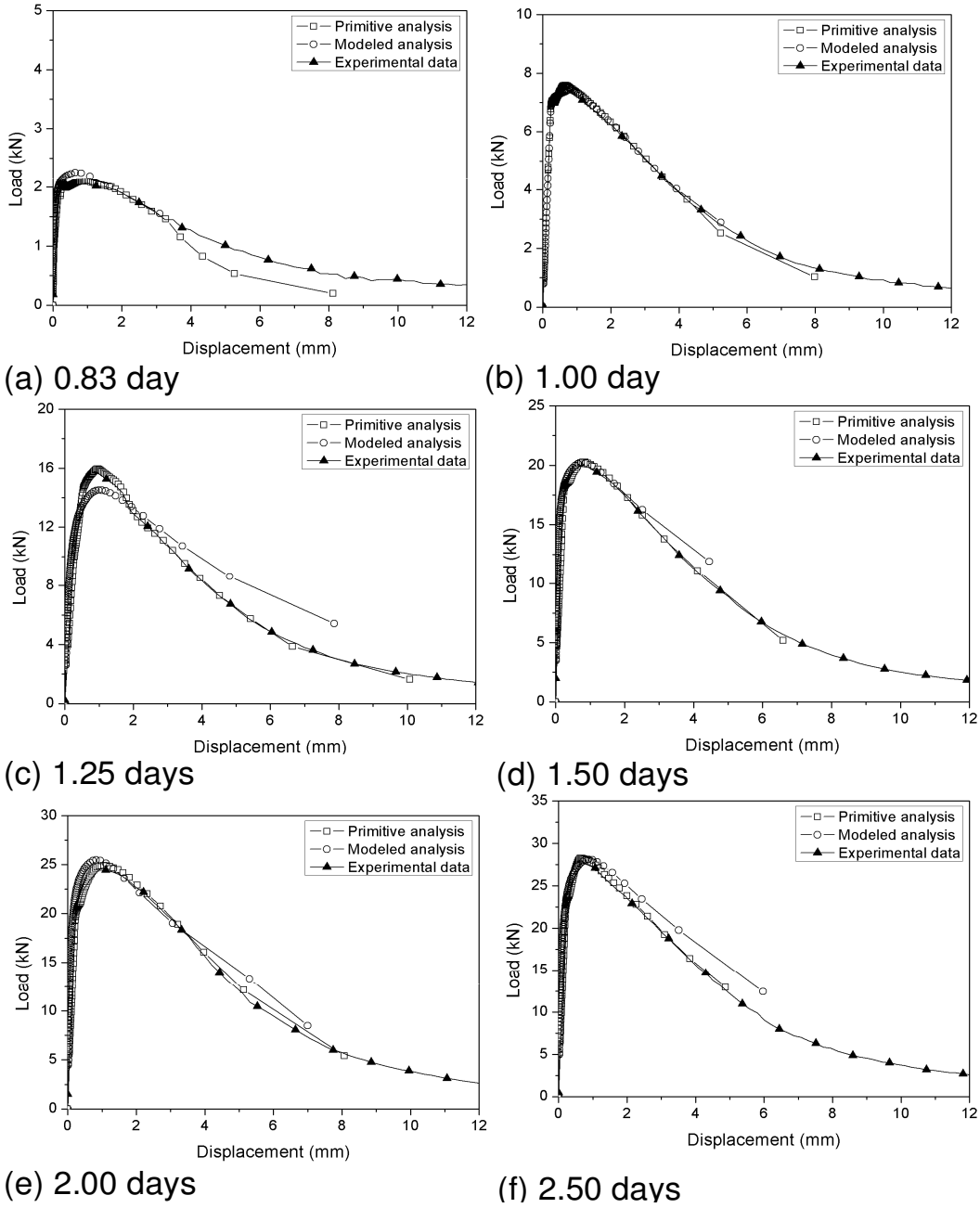

Figure 21. Comparisons of load-displacement curves (A-F).

$$\sigma_w = f_1 - \beta_d w \quad \text{for} \quad w_1 < w \le w_c \tag{8-2}$$

$$\sigma_w = 0 \quad \text{for} \quad w > w_c \tag{8-3}$$

The tensile softening curve, as modeled through the simplification process explained is considered to be very efficient in predicting the early crack growth and failure behavior of UHPFRC that displays strain-hardening behavior.

Verification of tensile softening model for air-cured UHPFRC at early ages

To verify the tensile softening model of air-cured UHPFRC at early ages, the load-displacement relationships derived from the simulation using primitive and modeled softening curves were compared with those obtained from the flexural tests. As shown in Figure 21, the primitive softening curves accurately simulated the load-displacement curves of the flexural tests. Although, it

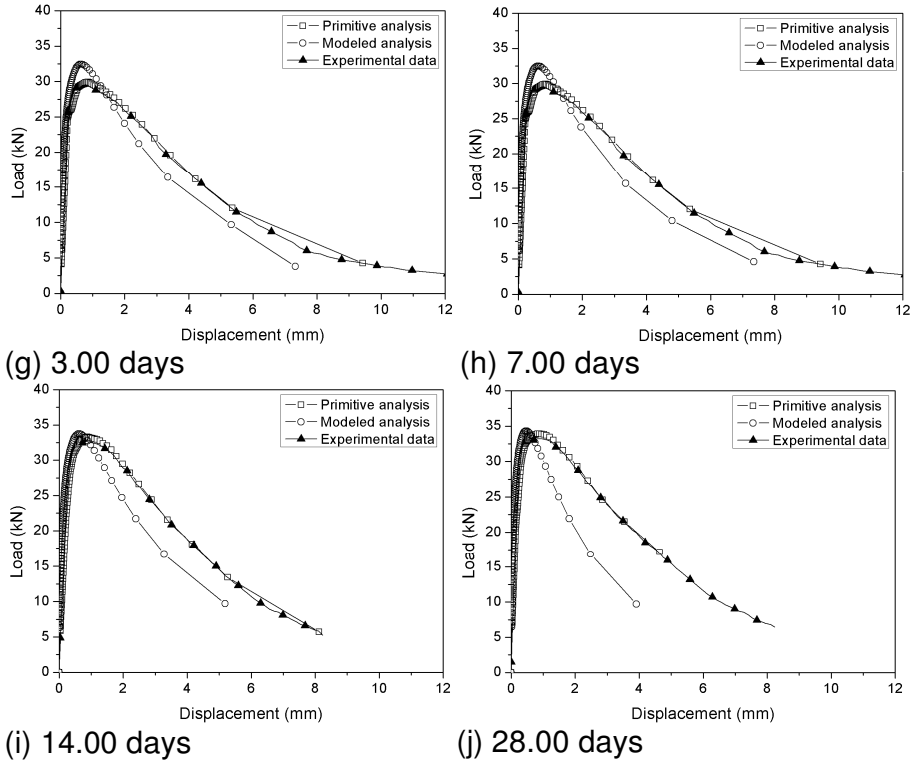

Figure 21. Comparisons of load-displacement curves (G-J).

is natural for the primitive softening curve to predict the test results more accurately than the modeled tensile softening curve, when the convenience of the modeled softening curve is considered, it also predicts the test results relatively accurately. Therefore, the modeled softening curve, can also be applied to effectively predicting the initial crack growth and failure behavior of structures constructed of UHPFRC.

Conclusions

This study considered the material properties of air-cured UHPFRC at early ages and proposed model equations based on test results to predict them. The conclusions gained through this study are as follows:

1. The compressive strength and modulus of elasticity of air-cured UHPFRC increased rapidly after 1.25 days, following the concrete casting. Based on the compressive test results, model equations for predicting the compressive strength and modulus of elasticity of UHPFRC at early ages were proposed.
2. The non-notched three-point flexural tests verified that, the flexural strength of UHPFRC manifested rapidly until the age of 3 days, and the strength at 7 days was almost equal to the strength at 28 days. Based on the flexural test results, a model equation for predicting the flexural strength of UHPFRC at early ages was proposed.
3. The compressive strength and modulus of elasticity of air-cured UHPFRC were about 64 and 84%, respectively, of those of high-temperature-cured UHPFRC, which is a substantial difference depending on the curing method. However, as the flexural strength of air-cured UHPFRC showed an 11% difference from that of high-temperature-cured UHPFRC, and the behavior in the post-peak region did not show a significant difference, the impact of the curing method on flexural performance was shown to be very slight.
4. The inverse analysis method was used to determine the tensile softening model for air-cured UHPFRC at early ages. A modeled softening curve that simplified the primitive softening curve derived from the inverse analysis, into two straight lines was proposed. Based on the simulation using the primitive and modeled softening lines, the load-displacement curves were compared with those measured from the notched flexural tests. The simulation results showed that, the modeled softening curve predicted the test results relatively well; thus, it can be used effectively in predicting the initial crack growth in structures constructed of UHPFRC.

REFERENCES

Bache HH (1987). Introduction to compact reinforced composite. Nordic Concr. Res., 6: 19–33.

Charron JP, Denarie E, Bruhwiler E (2004). Permeability of UHPFRC under high stresses. In: Proceedings RILEM symposium on advances in concrete through science and engineering, Chicago, USA, (CD-ROM).

Fehling E, Schmidt M, Teichmann T, Bunje K, Bornemann B (2004). Entwicklung, Dauerhaftigkeit und Berechnung Ultra-Hochfester Betone (UHPC) (Development, durability and calculation of ultra-high strength concretes (UHPC)). Res. Report, Schriftenreihe Baustoffe und Massivbau 1, Kassel. (in German).

Kang ST, Lee Y, Park YD, Kim JK (2010). Tensile fracture properties of an ultra high performance fiber reinforced concrete (UHPFRC) with steel fiber. Comp. Struct., 92: 61–71.

Katrin H, Marco V, Emmanuel D, Eugen-Habel B, Viviani M (2006). Development of the mechanical properties of an ultra-high performance fiber reinforced concrete (UHPFRC). Cement Concr. Res., 36: 1362–1370.

Kitsutaka Y (1995). Fracture parameters for concrete based on poly-linear approximation analysis of tension softening diagram, FRAMCOS-2, Germany, AEDIFICATION , pp. 199–208.

Kitsutaka Y, Kamimura K, Nakamura S (1993). Poly-linear approximation analysis of tension softening diagram for concrete. J. Struct. Constr. Engng. AIJ., 453: 15–25.

Lawler JS, Zampini D, Shah SP (2002). Permeability of cracked hybrid fiber-reinforced mortar under load. ACI Mater. J., 99(4): 379–385.

Origin version 7.5 (2003). On-line user's manual. (OriginLab, Inc.).

Parant E (2003). Mécanismes d'endommagement et comportements mécaniques d'un composite cimentaire fibré multi-échelles sous sollicitations sévères: fatigue, choc, corrosion (Damage mechanisms and mechanical behaviour of a cementitious composite with multi-scale fibre reinforcement under severe load conditions), Doctoral thesis, Laboratoire Central des Ponst et Chaussées, Paris, France, 2003 (in French).

Richard P, Cheyrezy M (1995). Composition of reactive powder concretes. Cement Concr Res., 25(7): 1501–1511.

Rossi P, Arca A, Parant E, Fakhri P (2005). Bending and compressive behaviors of a new cement composite. Cement Concr. Res., 35(1): 27–33.

Tanaka Y, Fukuura N, Uzawa T, SakaMoto J, Maehori S, Katagiri M (2005). Tensile characteristics and modeling of tension softening behavior for ultra high performance fiber-reinforced concrete. JSCE, 788(67): 159–173.

Uchida Y, Kurihara N, Rokugo K, Koyanagi W (1995). Determination of tension softening diagrams of various kinds of concrete by means of numerical analysis. FRAMCOS-2, Germany, AEDIFICATION, pp. 17–30.

Urs M, Birgit M, Hans-Carstan K, Jiri N, Patrick F (2008). Micro texture and mechanical properties of heat treated and autoclaved ultra high performance concrete (UHPC). In: Second Inter. Symp. on Ultra High Performance Concrete, Kassel University Press.